Supporting information for

Observation-based estimates of volume, heat and freshwater exchanges between the subpolar North Atlantic interior, its boundary currents and the atmosphere

Sam C. Jones[1], Neil J. Fraser[1], Stuart A. Cunningham[1], Alan D. Fox[1], Mark E. Inall[1]

[1]Scottish Association for Marine Science, Oban, UK

Correspondence to: Sam Jones (sam.jones@sams.ac.uk)

Contents of this file:

S1. Quality control and gridding of profile data

S2. Additional datasets

S3. Seasonal anomalies in boundary hydrography

S4. Diffusive heat flux

S5. Sub-1000 m transport correction

S6. Decomposition of heat and freshwater fluxes into overturning and along-isopycnal components

Introduction

The files included in the supplementary materials are additional text, figures and tables supporting the analysis presented in the article.

S1. Quality control and gridding of profile data

Here we detail additional quality controls applied to the profile data. The workflow is illustrated in Fig. S1.

S1.1 Local statistical range check

Profiles supplied by the WOD have already undergone a global range check, so we found no globally unphysical T and S values present in the data. However, a subset of profiles featured observations which were statistically unlikely for the latitude and longitude of the profile. To identify and remove these data, profiles were subset into 500 km segments by distance along the 1000 m contour. For each distance subset, we further subset into 50 dbar pressure brackets. For each pressure bracket, conservative temperature, absolute salinity and σ_0 values were computed. Any data falling outside 5 standard deviations of the mean were rejected. If more than 50 % of the profile was found to contain bad data, the whole profile was rejected.

S1.2 Density inversion test

We performed a simple density inversion test to identify and flag temperature and salinity profiles which resulted in density inversions. CT and SA profiles were binned onto a 20 dbar grid, and σ_0 recalculated. The profile was scanned for density inversions. If an inversion of > 0.03 kgm^{-3} was detected, the whole profile was rejected (Fig. S1).

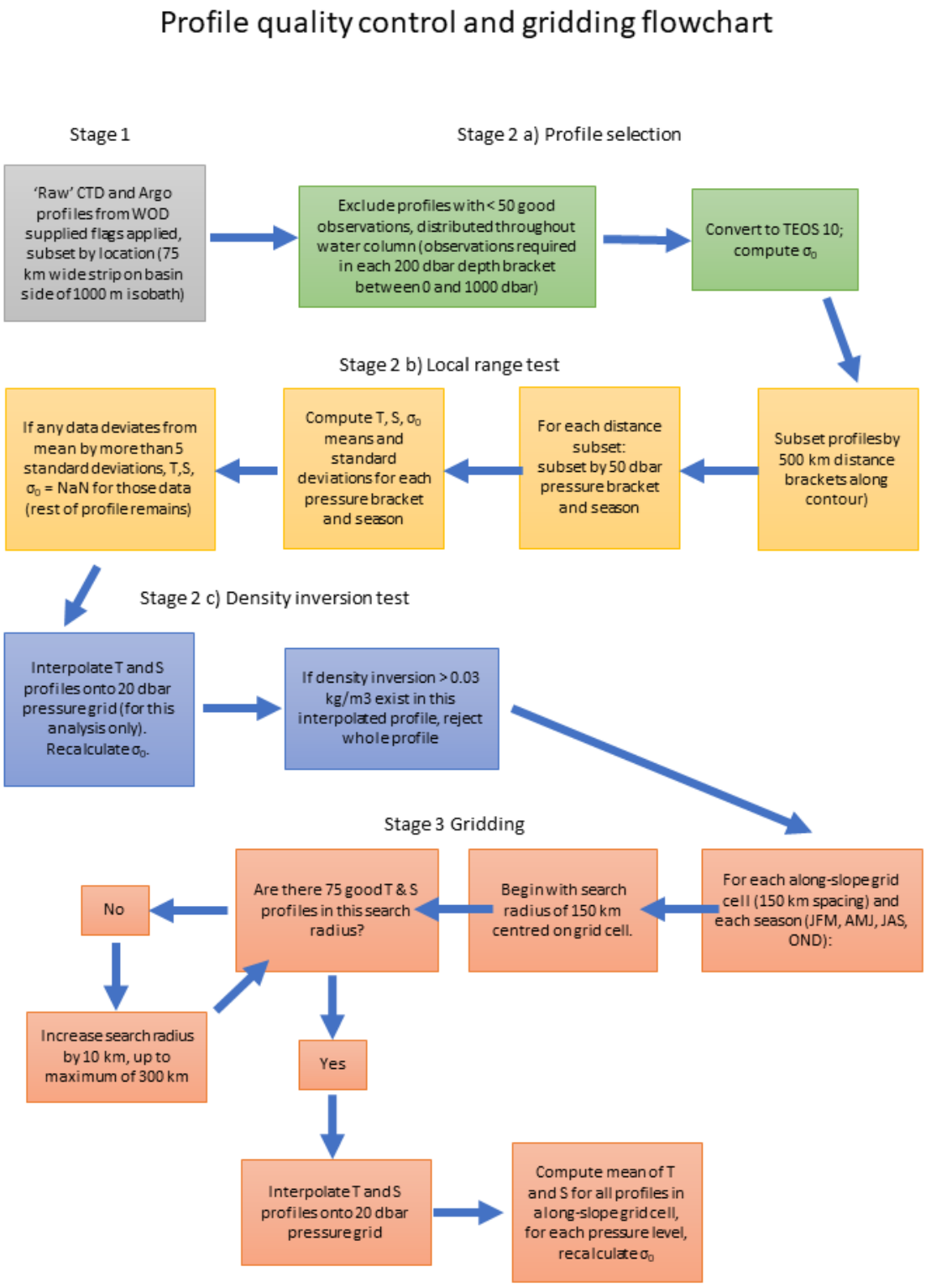

Figure S1: Flowchart of quality control and gridding method for Argo and CTD profile data.

S2. Additional datasets

Here we detail the acquisition of additional datasets necessary for the analysis.

S2.1. Satellite Absolute Dynamic Topography (ADT) data

Daily AVISO ADT data for the period 2000–2019 were downloaded from the Copernicus data server on 01/12/2020. (https://marine.copernicus.eu/, product identifier SEALEVEL_GLO_PHY_L4_REP_OBSERVATIONS_008_047). From these gridded data, ADT values were extracted at the locations of each mid-point station and temporally averaged for each season.

S2.2. GEBCO bathymetry

GEBCO 15 arcsecond gridded bathymetry data were acquired from https://www.gebco.net/ on 15/06/2020 (GEBCO Compilation Group, 2019).

S3. Seasonal anomalies in boundary hydrography

Figure S2 shows seasonal anomalies in temperature, salinity, density and velocity from the annual means depicted in Fig. 3.

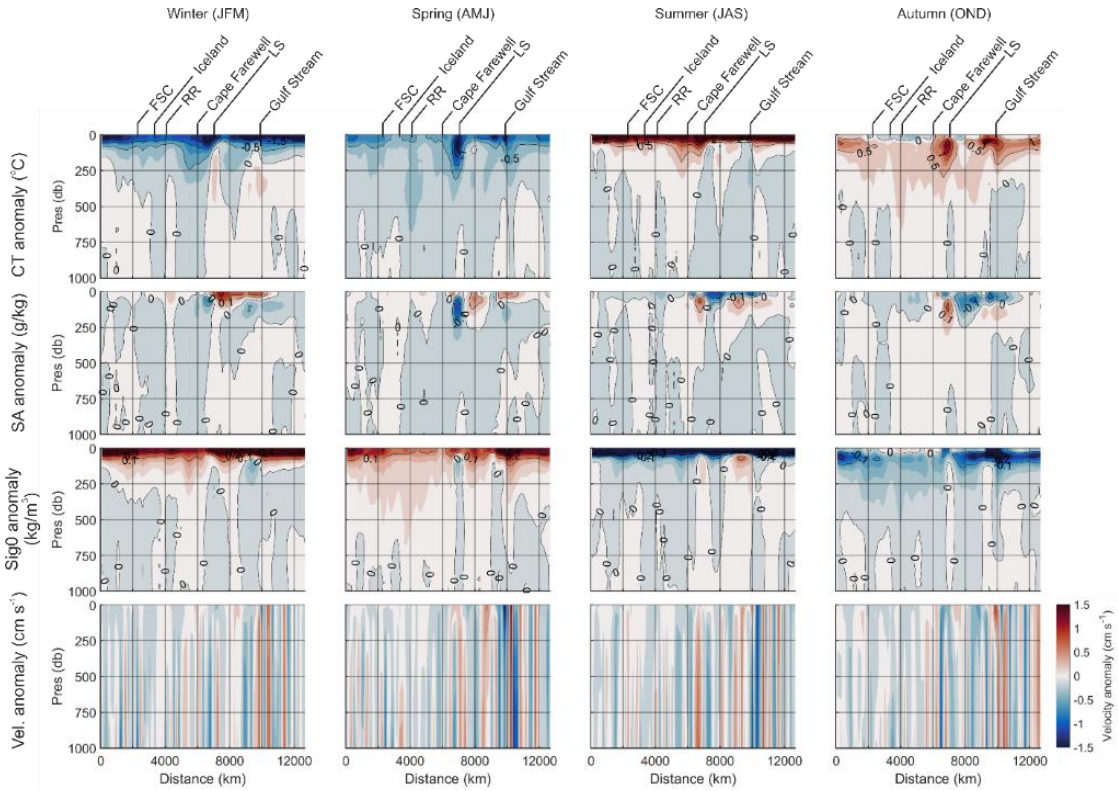

Figure S2: Seasonal anomalies: row 1) conservative temperature (℃), row 2) absolute salinity (g kg-1), row 3) density (σ0, kgm^{-3}), row 4) geostrophic velocities into the SPG, perpendicular to contour (cm s-1). Key locations around boundary labelled as for Fig. 3.

S4. Diffusive heat flux

Satellite derived SST and surface geostrophic velocities were obtained from the Copernicus data server for the year 2019 (see Sect. S2.1). These fields were interpolated onto the boundary contour and had a 150-day high-pass filter applied to leave only the fluctuating component of the fields. The 150-day filter length was chosen to remove the seasonal signal but retain the signal from larger eddies. The first normal baroclinic mode was computed from boundary density (Fig. 3) and used to model the structure of both the velocity and temperature fields, down to the first zero-crossing. The diffusive temperature flux vector was the computed by taking the time-mean of the product of the resulting temperature and velocity fields. The diffusive heat flux (per unit area) through boundary is the component of this vector perpendicular to the 1000 m contour multiplied by ρC_p= 4.1 W m^{-2}.

Figure S3 shows the accumulated diffusive heat flux moving anticlockwise around the boundary from the southeast corner. Heat is diffused out of the domain along the 1000 m contour, and into the domain along 47 °N. Around 0.025 PW enters in the gulf stream, but this is largely compensated by heat leaving the domain on either side. A total of 0.0062 PW of heat energy enters the domain via turbulent diffusion.

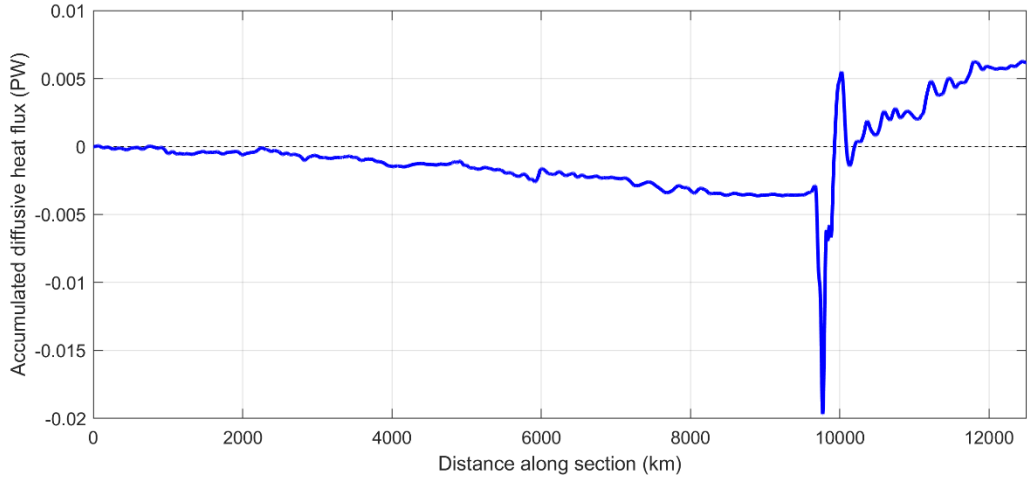

Figure S3: Diffusive heat flux accumulated around the boundary for 2019, based on satellite SST and surface geostrophic velocities. Positive values indicate heat entering the SPG at the boundary.

S5. Sub-1000 m transport correction

In this study we aim to provide an observation-based diagnosis of overturning and fluxes around the SPG boundary. However, temperature and salinity data derived from EN4 lack the resolution to capture the strong and small-scale baroclinic shears associated with the Gulf Stream and the deep western boundary current. As geostrophic velocities are referenced to SSH this leads to the Gulf Stream failing to diminish with depth, and a resultant overestimation of transport into the domain (Fig. S4, Fig. S5).

For the computation of fluxes and overturning, we require full depth, mass-balanced velocities across 47 °N. We consider the use of model data for this section to be contrary to the ethos of this study, which is to provide a budgetary estimation of the SPG with as few preconceptions as possible.

We aim to preserve the geostrophic velocities above 1000 m, so a possible solution is to compute a reference velocity for the sub-1000 m region (labelled B, Fig. S4), that when added to this region balances the transports entering and leaving the volume. While this approach results in net zero transport into the domain, the Gulf Stream remains substantially larger than observed in nature (illustrated by the model transect in Fig. S4a).

To partially remedy this discrepancy, we perform a 2-stage velocity correction. First, we apply a linear multiplier to the Gulf Stream and the adjacent retroflection, ranging from 1 at 1000 m to 0 at the seabed (Region A, Fig. S4). Second, we apply the mass-balanced velocity correction to the full sub-1000 m region (region B, Fig. S4) as before. The impact on cumulative transports is shown in Fig. S5. We consider this approach to provide estimates of fluxes and overturning which best preserve the observations, but which are underpinned by more physically plausible transports in sub-1000 m water across 47 °N. As most strong property gradients are above 1000 m the results are quite robust to this correction, but its impact on the results is highlighted where appropriate. Note in particular the hatched areas in Figs. 4 and 9. In addition, the impact of the velocity correction on the cumulative heat and freshwater fluxes is shown in Fig. S6.

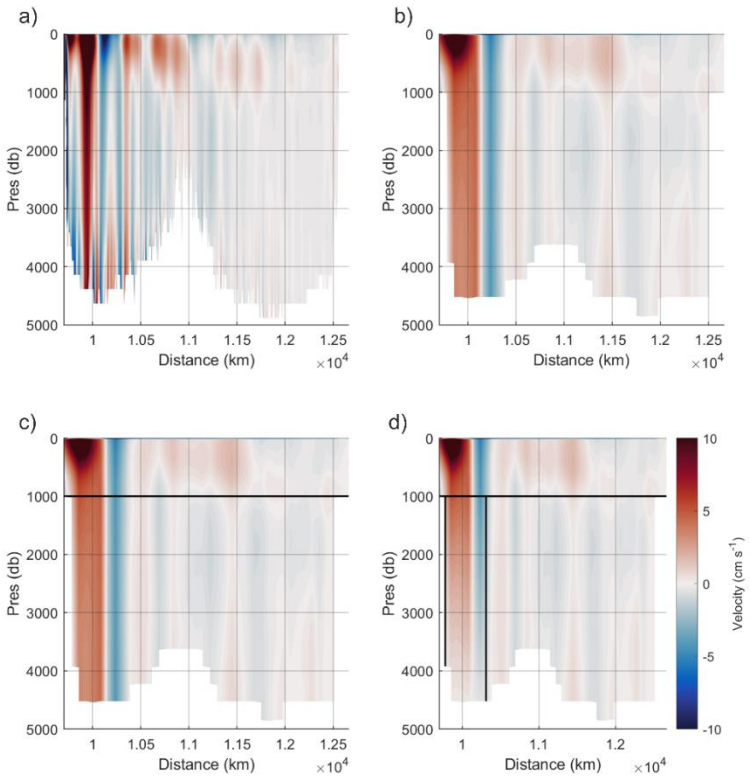

Figure S4: Full-depth velocities across 47 °N a) in VIKING20X, 2000-2018 mean b) Surface-referenced observed geostrophic + surface Ekman velocities, no correction, c) as before, but with sub-1000 m mass-balanced velocity correction only, d) As before, but with Gulf Stream reduction towards seabed and mass-balanced velocity correction.

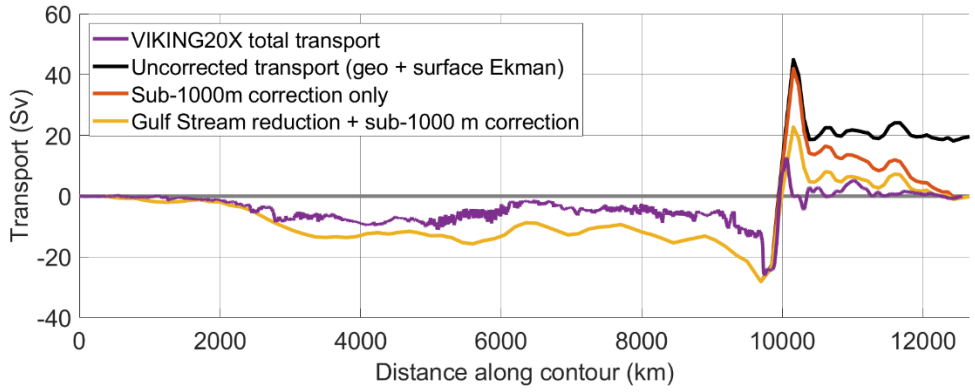

Figure S5: Annual mean cumulative transports around the SPG boundary between surface and seabed, showing VIKING20X total transport (purple) compared to: observation-based transports resulting from uncorrected velocities (black), observation-based transports with a simple volume flux correction below 1000 m (orange) and observation-based transports with a 2-stage correction to first reduce the Gulf Stream with depth, then balance volume fluxes (yellow).

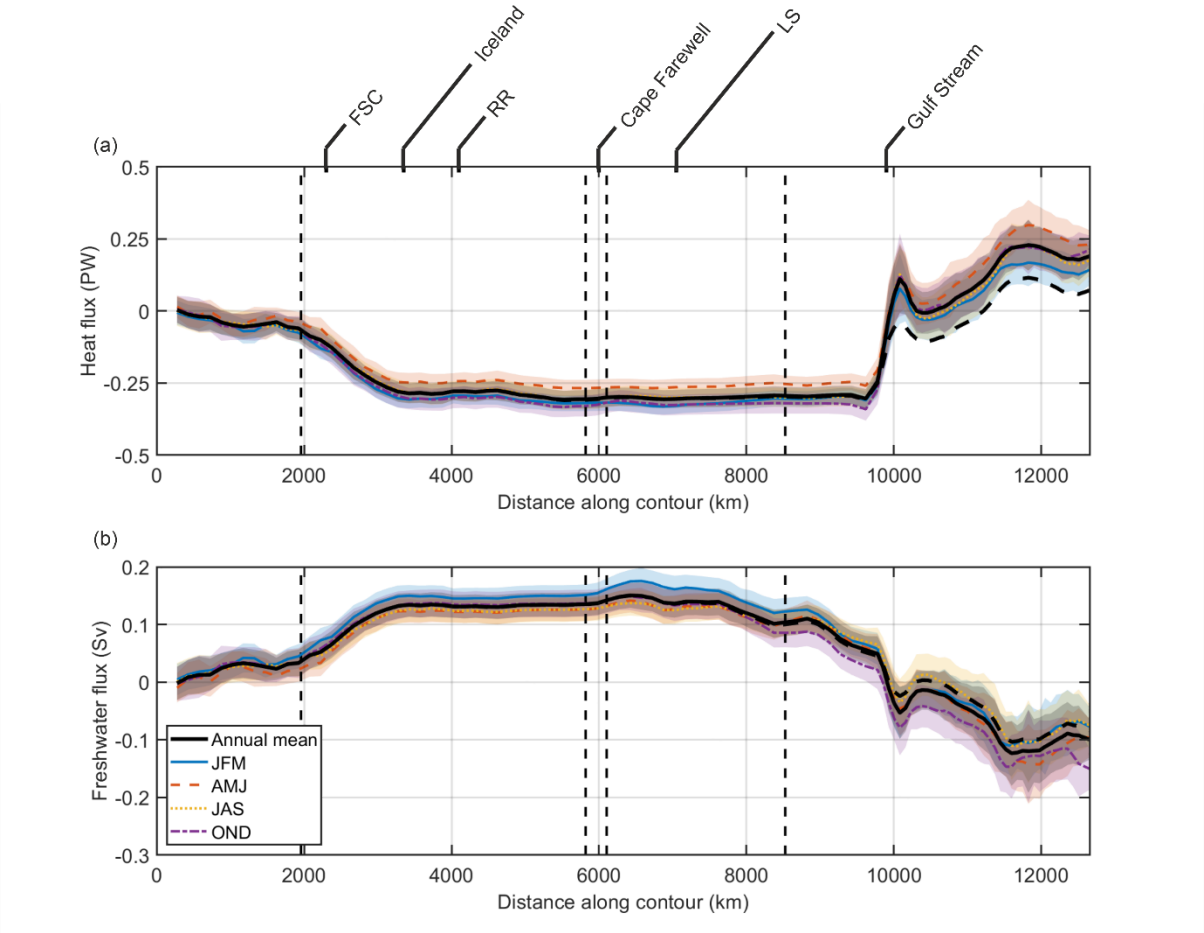

Figure S6: Cumulative heat [PW] and fresh-water [Sv] fluxes into the SPG between surface and seabed for a) heat and b) freshwater, using corrected velocities for sub-1000 m currents. Heavy dashed black line shows annual mean fluxes using uncorrected velocities.

S6. Decomposition of heat and freshwater fluxes into overturning and along-isopycnal components

Heat and freshwater fluxes are decomposed into their overturning and along-isopycnal components in density space by first defining the total velocity, conservative temperature, and absolute salinity as:

$$v(x,\sigma) = < v > (\sigma) + v'^{(x,\sigma)} [m\ s^{-1}] \quad (S1)$$

$$\theta(x,\sigma) = < \theta > (\sigma) + \theta'^{(x,\sigma)} [^{\circ}C] \quad (S2)$$

$$S(x,\sigma) = < S > (\sigma) + S'^{(x,\sigma)}\ [kg\ m^{-3}] \quad (S3)$$

Where the angle brackets denote a horizontal average at constant density and prime indicates deviations from that average. The heat flux can be divided into an 'overturning' ($Q_{\theta\_overturning}$) and 'along isopycnal' component ($Q_{\theta\_isopycnal}$), where the factor $\frac{\partial z}{\partial \sigma}$ is required to change variable from depth space to density space:

$$Q_{\theta_{overturning}} = \rho C_p \int_{\sigma_{min}}^{\sigma} \int_{x_{end}}^{x_{start}} < v > (< \theta > - \bar{\theta}) \frac{\partial z}{\partial \sigma} dx d\sigma\ [W] \quad (S4)$$

$$Q_{\theta_{isopycnal}} = \rho C_p \int_{\sigma_{min}}^{\sigma} \int_{x_{end}}^{x_{start}} v' \theta' \frac{\partial z}{\partial \sigma} dx d\sigma\ [W] \quad (S5)$$

The freshwater flux is also decomposed thus:

$$Q_{f\_overturning} = - \int_{\sigma_{min}}^{\sigma} \int_{x_{end}}^{x_{start}} < v > \frac{< S > - \bar{S}}{\bar{S}} \frac{\partial z}{\partial \sigma} dx d\sigma\ [Sv] \quad (S6)$$

$$Q_{f_{isopycnal}} = - \int_{\sigma_{min}}^{\sigma} \int_{x_{end}}^{x_{start}} v' \frac{S'}{\bar{S}} dx d\sigma\ [Sv] \quad (S7)$$

Decomposed heat and freshwater fluxes are shown in Table S1.

Table S1: Net fluxes into SPG [between surface and seabed]

	Heat [PW]			**Freshwater [Sv]**		
	Total	**Overturning**	**Along-isopycnal**	**Total**	**Overturning**	**Along-isopycnal**
Annual mean	0.18 ± 0.05	0.14 ± 0.05	0.04 ± 0.04	-0.10 ± 0.03	-0.06 ± 0.02	-0.04 ± 0.03
JFM	0.14 ± 0.05	0.13 ± 0.05	0.02 ± 0.04	-0.08 ± 0.02	-0.08 ± 0.02	0.01 ± 0.03
AMJ	0.23 ± 0.05	0.22 ± 0.05	0.01 ± 0.04	-0.10 ± 0.02	-0.10 ± 0.03	0.01 ± 0.04
JAS	0.17 ± 0.05	0.16 ± 0.05	0.01 ± 0.05	-0.07 ± 0.02	-0.07 ± 0.03	0.01 ± 0.03
OND	0.21 ± 0.05	0.13 ± 0.05	0.09 ± 0.05	-0.15 ± 0.02	-0.04 ± 0.03	-0.10 ± 0.04